Probabilistic Available Transfer Capability Assessment in Power Systems with Wind Power Integration

Xin Sun [1], Zhongbei Tian [2*], Yufei Rao [1], Zhaohui Li [1], Pietro Tricoli [2]

[1] Electric Power Research Institute, State Grid Henan Company, Zhengzhou, People's Republic of China
[2] Department of Electronic, Electrical and Systems Engineering, University of Birmingham, Birmingham, UK
[*] z.tian@bham.ac.uk

Abstract: Extending current deterministic tools to incorporate significant stochastic wind power is becoming an important as well as challenging task for present-day power system decision-making. This paper proposes a novel probabilistic assessment method to assess the available transfer capability (ATC). Usually, a large number of ATC evaluations is needed to obtain accurate results using time-consuming Monte Carlo simulations (MCS). To alleviate the computation burden of probabilistic ATC, a statistically-equivalent surrogate model for the ATC solution is constructed by introducing canonical low-rank approximation (LRA). By implementing LRA for the base case and a set of enumerated contingencies, the uncertainties of wind power generation and load, as well as transmission equipment outages, are addressed in an efficient way. With the proposed method, the probability of ATC is characterised, and the most influential uncertain factors are identified, which helps to determine a suitable ATC level. The effectiveness of the proposed method is validated via case studies with a modified IEEE 118-bus system.

1. Introduction

The exploitation and utilisation of wind power are regarded as an effective way to tackle the challenges of climate change and the energy crisis. Due to its stochastic nature, the actual wind power generation can vary significantly from its scheduled value [1]. In order to integrate a high proportion of wind power into power systems, there is a pressing need to quantify the impact of its uncertainty on power system operation indices and, hence, ensure a secure and reliable transmission network. In order to utilise the transmission network rationally, the North American Electric Reliability Corporation (NERC) has defined the available transfer capability (ATC) as a measure of the power transfer capability remaining in the transmission network for further commercial activities over and above already-committed uses [2]. It quantifies the amount of power in MW that can be exchanged between areas without violating any security constraints in both pre- and post-contingency conditions. For electricity market participants, the information on the ATC serves as a reference for designing purchase and sale contracts, while for system operators, the precalculated ATC value can be used as a security indicator of the transmission infrastructure.

Conventionally, ATC is evaluated by a deterministic approach, for instance, sensitivity-based power flow [3], continuation power flow (CPF) [4], repeated power flow (RPF) [5] and optimal power flow (OPF) [6]. It is widely recognised that the ATC calculation should accommodate reasonable uncertainties in the system conditions to guarantee flexible and reliable system operations [2]. In a power system with a significant proportion of wind power generation, where the principle of addressing uncertainty attracts more attention, probabilistic ATC calculation is considered to be more promising than deterministic methods [7-10]. Monte Carlo simulations (MCS) are widely used for assessing probabilistic ATC [11-14]. Even though the stochastic behaviors of ATC can be accurately characterized, the application of MCS to time-sensitive cases is not technically feasible due to it involves a huge number of ATC evaluations for the randomly sampled states to reach convergence. The efficiency of MCS can be improved by adopting variance reduction techniques that reduce the number of trials [15-16]. In recent years, polynomial chaos expansion (PCE) has been proved as a promising solution to alleviate the computation burden of MCS [17-18]. In PCE, a surrogate model for generating ATC samples is built up by a series expansion of multivariate orthogonal polynomials, and the probabilistic ATC evaluation is accelerated due to the simulations on the time-consuming original model are reduced. However, the necessary number of original model simulations increases exponentially with the dimension of inputs [19], which makes the efficiency merit of PCE disappears in those practical power system problems involving a great number of uncertain parameters concerning loads, generations and others. Besides MCS and PCE, small-sample methods, like

Table 1 Probabilistic ATC methods comparison

Method	Attractive points	Defects
MCS	It is accurate to characterize the stochastic behaviors of ATC.	Heavy computation burden is involved to reach convergence.
PCE	It saves computation effort of MCS by employing a surrogate model to generate random samples of ATC.	The advantage of efficiency disappears in high-dimensional applications.
PEM	It carries out a few deterministic routines with selected points to estimate the statistical moments of ATC.	The accuracy of series expansion to estimate the probability distribution of ATC is not guaranteed.
bootstrap	The statistical moments of ATC are estimated by repeated sampling from historical data.	It is difficult to guarantee the validity of the results depending on the selected ATC samples.

point estimation methods (PEM) [20] and bootstrap methods [21], require fewer random samples of ATC but extra mathematical treatments. Although the computational effort is attractive, small-sample methods are not always accurate enough. For example, PEM would have bad performance when selecting unsuitable series to fit the probability distributions of random variables [22]. The pros and cons of these methods are summarized and compared in Table 1. In general, a probabilistic ATC method ensuring both accuracy and efficiency is still in need.

Besides the aforementioned concern, the probabilistic ATC framework could be further improved by providing information about which uncertain factors would have the greatest effect on ATC variation. Such uncertainty importance measure can help to identify random variables or parameters needed for improved forecast or modelling, so that more reliable probabilistic ATC results can be provided [23]. Moreover, the quantification of uncertainty importance can also guide system operators towards taking effective control actions, for example installing energy storage next to important renewable energy plants identified to mitigate the ATC variability [24]. Several uncertainty importance measures are investigated in ref. [25], among which variance-based global sensitivity analysis (GSA) is recognized as an applicable one in the context of power system. Because GSA is conducted with a large number of structural samples of random inputs [26], its computational burden has become a concern and prohibited its applications to problems including the ATC assessment.

This paper addresses the needs above by developing a novel probabilistic ATC calculation method based on the low-rank approximation (LRA) technique. LRA offers a promising alternative to PCE for developing surrogate models based on the idea of canonical decompositions [27]. The canonical decompositions are typically used to compress and extract information of a tensor and have been used in a broad range of fields, like signal processing and data mining [28-30]. Recently, it also attracts interest in the probabilistic power flow problem [31]. The number of coefficients in canonical decompositions grows linearly rather than exponentially with the input dimension [32], making LRA more powerful in dealing with high-dimensional problems. The main benefits of the proposed method are:

i. Under the base case and a set of transmission contingency cases, the LRA representation for the ATC solution is built and used as a surrogate model to calculate ATC coping with uncertain load and wind power.
ii. The statistics and probability distributions of ATC, as well as the global sensitivity index (GSI) of random input are expressed according to the law of total probability, by which the discrete-distributed transmission status are analytically handled.

Consequently, the proposed method improves the efficiency of the probabilistic ATC calculation while ensuring high accuracy.

The remainder of the paper is organised as follows. The problem formulation of the probabilistic ATC calculation is provided in Section 2. Section 3 describes the implementation procedure of the canonical LRA. Section 4 presents the realisation of the LRA-based probabilistic ATC assessment in detail, followed by numerical case studies on a modified IEEE 118-bus system in Section 5. Conclusions are drawn in Section 6.

2. Probabilistic ATC Assessment

2.1. Mathematical formulation for ATC

According to the NERC definition, ATC can be expressed as the total transfer capability (TTC) less the transmission reliability margin (TRM), less the sum of existing transmission commitments (ETC) and the capacity benefit margin (CBM), that is:

$$ATC = TTC - TRM - (ETC + CBM) \tag{1}$$

where *TTC* indicates the maximum MW power that can be transferred over the transmission network without violating the security constraints for a set of defined pre- and post-contingency conditions; *ETC* is determined for a specific base case, which is a system operating state determined by parameters including load demands, generation outputs and network configurations, etc; *TRM* is defined as the amount of transfer capability necessary to ensure the reliable and secure operation of transmission networks under a range of uncertainties in system conditions; *CBM* is a locally applied margin reserved by load-serving entities to ensure access to generation from elsewhere in the interconnected systems to meet generation reliability requirements.

In practice, TRM and CBM, as two transfer capability margins, are usually treated as fixed values or percentages of TTC to meet specific reliability requirements and are therefore neglected in some ATC calculation methods for simplicity [33]. In this paper, the determination of TRM is addressed in the probabilistic ATC scheme to accommodate the wind power uncertainty. It will be discussed in section 4.

The ATC calculation for a deterministic case, e.g., the base case, can be expressed by the mathematical formulation below:

$$\begin{aligned} &\text{Min} \ -f(\boldsymbol{u}) \\ &\textit{subject to} \\ &\boldsymbol{g}(\boldsymbol{u})=0, \quad \boldsymbol{h}(\boldsymbol{u}) \le 0 \end{aligned} \tag{2}$$

where $\boldsymbol{u}$ denotes the vector of the state and control variables. The model objective $f(\boldsymbol{u})$ is to maximize the active power transferred through a transmission network or line without compromising system security, i.e., satisfying the constraints on $\boldsymbol{g}(\boldsymbol{u})$ and $\boldsymbol{h}(\boldsymbol{u})$.

2.2. OPF based deterministic ATC evaluation

In this paper, the OPF model incorporating the thermal and voltage security limits is used as the ATC calculator. Moreover, it is not difficult to include the dynamic stability limits by implementing the stability-constrained optimal power flow (SCOPF). In SCOPF, dynamic equations are converted to numerically equivalent algebraic equations and then integrated into the standard OPF formulation [34].

Specifically, the OPF objective function $f(\boldsymbol{u})$ is expressed as:

$$f(\boldsymbol{u}) = \sum_{i \in \boldsymbol{SE}} \left(P_{\mathrm{G}i} - P_{\mathrm{G}i,0} \right) \tag{3}$$

The equality constraints $\boldsymbol{g}(\boldsymbol{u})$ include:

1) the physical power flow equations:

$$\begin{cases} P_{\mathrm{G}i} + P_{\mathrm{W}i} - P_{\mathrm{D}i} - V_i \sum_{j \in i} V_j \left(G_{ij} \cos\theta_{ij} + B_{ij} \sin\theta_{ij} \right) = 0 \\ Q_{\mathrm{G}i} + Q_{\mathrm{W}i} - Q_{\mathrm{D}i} - V_i \sum_{j \in i} V_j \left(G_{ij} \sin\theta_{ij} - B_{ij} \cos\theta_{ij} \right) = 0 \end{cases} \tag{4}$$

2) the load increase pattern:

$$P_{\mathrm{D}i} - P_{\mathrm{D}i,0} = \lambda b_{\mathrm{D}i}, \quad Q_{\mathrm{D}i} / P_{\mathrm{D}i} = Q_{\mathrm{D}i,0} / P_{\mathrm{D}i,0} \tag{5}$$

The inequality constraints $\boldsymbol{h}(\boldsymbol{u})$ include:

3) the generation capacity limits:

$$P_{\mathrm{G}i,\min} \le P_{\mathrm{G}i} \le P_{\mathrm{G}i,\max}, \, i \in \boldsymbol{SE} \tag{6}$$

$$P_{\mathrm{G}i} = P_{\mathrm{G}i,0}, \, i \notin \boldsymbol{SE} \tag{7}$$

$$Q_{\mathrm{G}i,\min} \le Q_{\mathrm{G}i} \le Q_{\mathrm{G}i,\max}, \; \forall i \tag{8}$$

4) the load demand limits

$$b_{\mathrm{D}i,0} \ge 0, \; i \in \boldsymbol{SI}, \quad b_{\mathrm{D}i,0} = 0, \; i \notin \boldsymbol{SI} \tag{9}$$

5) the voltage limits:

$$V_{i,\min} \le V_i \le V_{i,\max}, \; \forall i \tag{10}$$

6) the thermal limits

$$P_{\mathrm{L}ij}^2 + Q_{\mathrm{L}ij}^2 \le S_{\mathrm{L}ij,\max}^2, \; \forall ij \tag{11}$$

where $P_{\mathrm{G}i}$ and $Q_{\mathrm{G}i}$ are the active and reactive generations; $P_{\mathrm{D}i}$ and $Q_{\mathrm{D}i}$ are the active and reactive load demands at bus i in the maximum-transfer case, respectively; $P_{\mathrm{G}i,0}$, $P_{\mathrm{D}i,0}$ and $Q_{\mathrm{D}i,0}$ are those in the base case; $P_{\mathrm{G}i,\min}$ and $Q_{\mathrm{G}i,\min}$, and $P_{\mathrm{G}i,\max}$ and $Q_{\mathrm{G}i,\max}$ are the lower and upper bounds of the active and reactive generations at bus i, respectively; $P_{\mathrm{W}i}$ and $Q_{\mathrm{W}i}$ are active and reactive wind generation, that remain unchanged in the base and maximum-transfer cases because wind power is non-dispatchable; λ is a scalar parameter representing the load increment; $b_{\mathrm{D}i}$ is the constant specifying the load increase rate; V_i and θ_i are the voltage magnitude and angle of bus i; $\theta_{ij} = \theta_i - \theta_j$; G_{ij} and B_{ij} are the elements of the system admittance matrix; $V_{i,\min}$ and $V_{i,\max}$ are the lower and upper bounds of V_i; $P_{\mathrm{L}ij}$ and $Q_{\mathrm{L}ij}$ are the active and reactive power on line i–j; and $S_{\mathrm{L}ij,\max}$ is its apparent power capacity. $\boldsymbol{SE}$ and $\boldsymbol{SI}$ are the set of buses in the source and sink areas.

With the OPF model above, the maximum-transfer case is established by solving the constrained nonlinear programming problem that provides the ATC of the transmission network.

2.3. Probabilistic ATC using surrogate model

The statistical and probabilistic properties of ATC are evaluated by the probabilistic method. Typically, it can be realised by the MCS procedure:

i. Generate N_{sim} samples for wind generation, loads and network topologies by random sampling
ii. Execute deterministic model simulation to evaluate ATC for each sample
iii. Get statistics and probability distributions of ATC.

The procedure above is quite time-consuming since a large number of repeated simulations is needed to achieve convergence so that a reliable result is obtained. The iteration can be terminated when $\sigma_{\mathrm{MCS}} / \sqrt{N_{\mathrm{sim}}}$ is smaller than a specified level, where σ_{MCS} is the standard deviation of ATC. It provides a rule to decide whether the amount of simulations is sufficient or not.

In order to improve the MCS-based probabilistic method, it is proposed to take advantage of a statistically-equivalent surrogate model which is able to predict the ATC solutions with less computation effort. This procedure is illustrated in Fig. 1. The surrogate model, i.e., PCE or LRA, is built with results of a few rounds of deterministic ATC simulations in the first stage, and used for generating enough ATC samples subsequently in the second stage. Because N_{ed} is far less than N_{sim}, the computation burden of the probabilistic ATC assessment is greatly alleviated.

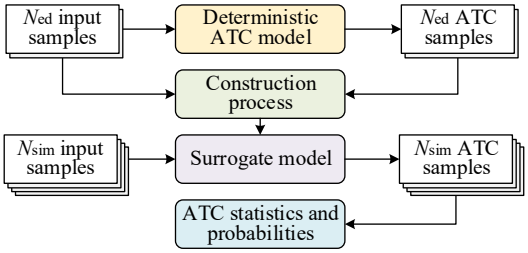

Fig. 1. *Probabilistic ATC assessment with surrogate model*

3. Canonical Low-Rank Approximation

In this section, the general form for the canonical low-rank representation of a computation model in the stochastic space is presented. Typically, it consists of four parts, as follows.

3.1. Representation of input random variables

In this step, the uncertainty sources are expressed in terms of the standard random variables (SRVs) $\boldsymbol{\xi}$, e.g., Gaussian, Beta, Uniform, etc. The SRVs are statistically independent. However, the random variables modeling the uncertainties in the physical system, $\boldsymbol{X} = [X_1, \ldots, X_n]^{\mathrm{T}}$ might be correlated. To address the correlation issue, the copula theory [35] is employed in this paper.

According to Sklar's theorem, the joint distribution of $\boldsymbol{X}$ can be expressed as:

$$F_{\boldsymbol{X}}(\boldsymbol{x}) = Cp(F_1(x_1), \cdots, F_n(x_n)) \tag{12}$$

where $F_{\boldsymbol{X}}$ is the joint cumulative distribution function (CDF) of $\boldsymbol{X}$, F_i is the marginal CDF of X_i, and Cp denotes the copula function.

Then, the correlated random variables are modeled by:

iv. Determining the marginal distributions for each and every random variable X_i
v. Selecting a suitable copula function to represent the dependence structure of multiple random variables $\boldsymbol{X}$
vi. Expressing $\boldsymbol{X}$ in terms of SRVs $\boldsymbol{\xi}$ with the principle of equal probability

Consequently, the invertible transformation between $\boldsymbol{X}$ and $\boldsymbol{\xi}$ is established and denoted as $\boldsymbol{\xi} = T(\boldsymbol{X})$.

3.2. Low-rank Approximation with Polynomial Basis

For a computation model in the stochastic space, its output response Y can be approximately represented by a sum of rank-one functions:

$$Y = M(\boldsymbol{\xi}) \approx \sum_{l=1}^{r} b_l w_l(\boldsymbol{\xi}) \tag{13}$$

where scalars b_l, $l = 1, \ldots, r$, are normalising factors, and w_l is the l-th rank-one function of $\boldsymbol{\xi}$ in the form of:

$$w_l(\boldsymbol{\xi}) = \prod_{i=1}^{n} v_l^{(i)}(\xi_i) \tag{14}$$

where $v_l{}^{(i)}$ denotes the i-th dimensional univariate function in the l-th rank-one function.

The right-hand side of (13) constitutes a canonical rank-r decomposition of the original model which might not be unique. It is usually of interest to find a decomposition consisting of a small number of terms that approximates the output response with sufficient accuracy, which is known as the canonical LRA.

The LRA expressed by (13) is further realised by expanding $v_l^{(i)}$ onto an orthogonal polynomial basis:

$$Y \approx \hat{M}_r(\boldsymbol{\xi}) = \sum_{l=1}^{r} b_l [\prod_{i=1}^{n} (\sum_{k=0}^{p_i} z_{k,l}^{(i)} \phi_k^{(i)}(\xi_i))] \quad (15)$$

where $\phi_k^{(i)}$, $k = 0, \ldots, p_i$, denotes the k-th degree univariate polynomial of the i-th input random variable ξ_i, and $z_{k,l}^{(i)}$ is the expansion coefficient of $\phi_k^{(i)}$ in the l-th rank-one function w_l.

The univariate polynomials $\phi_k^{(i)}$ are selected according to the marginal probability distribution of ξ_i, for example, Hermite polynomials for a Gaussian distribution, Legendre polynomials for a uniform distribution, and Jacobi polynomials for a Beta distribution [36].

3.3. Estimation of Model Constants

When the approximation model has been built in the form of (15), the undetermined constants, including the normalizing factors $\{b_1, \ldots, b_r\}$ and the polynomial coefficients $\{ z_{k,l}^{(i)} \mid i = 1, \ldots, n, k = 0, \ldots, p_i, l = 1, \ldots, r\}$, are solved as following.

Firstly, a set of SRV samples $\boldsymbol{\xi}_{\text{ed}} = \{\boldsymbol{\xi}^{(1)}, \ldots, \boldsymbol{\xi}^{(N\text{ed})}\}$, termed as the experimental design (ED), are randomly generated based on the joint probability distribution of $\boldsymbol{X}$, and the corresponding responses $\boldsymbol{y}_{\text{ed}} = \{y^{(1)}, \ldots, y^{(N\text{ed})}\}$ are evaluated by the original model, i.e., $y^{(i)} = M(\boldsymbol{\xi}^{(i)})$, $i = 1, \ldots, N_{\text{ed}}$.

Then, a sequence of pairs of correction-updating operators is performed, so that the approximation model with the solved normalising factors and polynomial coefficients is accurate enough to represent the original model concerning the ED samples. Specifically:

1) In the t-th correction step, a new rank-one function w_t is formed and added into the approximation model to minimize the residue of Y at the (t−1)-th step:

$$w_t(\boldsymbol{X}) = \arg \min_{w \in W} \sum_{m=1}^{N_{\text{ed}}} [y^{(m)} - \hat{M}_{t-1}(\boldsymbol{\xi}^{(m)}) - w(\boldsymbol{\xi}^{(m)})]^2 \quad (16)$$

2) In the t-th updating step, the existing normalizing factors $\boldsymbol{b} = [b_1, \ldots, b_t]$ are determined by solving the minimization problem below:

$$\boldsymbol{b} = \arg \min_{\boldsymbol{\beta} \in R^t} \sum_{m=1}^{N_{\text{ed}}} [y^{(m)} - \sum_{l=1}^{t} \beta_l w_l(\boldsymbol{\xi}^{(m)})]^2 \quad (17)$$

The details of the solution process above are discussed in the literature [32] and omitted in this paper. However, it is worth mentioning here that LRA has two attractive features:

i. The unknown constants to be estimated grow linearly with the dimension n of input random variables, i.e., r normalizing factors and $r \cdot \Sigma n$ i=1(p_i+1) polynomial coefficients;
ii. Only a series of small-size least-square regressions are involved in estimating the unknown constants in the sequential correction-updating scheme.

3.4. Discussion

So far, the LRA model is constructed based on the given parameters, i.e., rank r, polynomial degree p_i and ED size N_{ed}. The criteria for selection of the optimal parameters is not yet well established. In the existing literature, one solution is to specify a candidate set of parameters firstly, e.g., {1, 2, 3, 4, 5} for r and {2, 3, 4, 5} for p_i. Then, the parameter selection is performed by progressively increasing the parameter and applying the error-based measure to select the best one [31]. The ED set is deemed insufficient if the final error measure is greater than a prescribed threshold, and should be enriched for a new investigation. It has been illustrated that the LRA with improper parameters would not predict the model response correctly [32], and therefore, leads to the invalid results. Although it seems setting r = 1or 2, and p_i = 2 or 3, would be an appropriate choice for engineering applications, the optimal parameter selection is still an open question that calls for further investigations.

4. Probabilistic ATC Assessment Based on LRA

In this section, a probabilistic ATC method is developed by introducing LRA into the assessment scheme. The whole procedure has three stages as shown in Fig. 2.

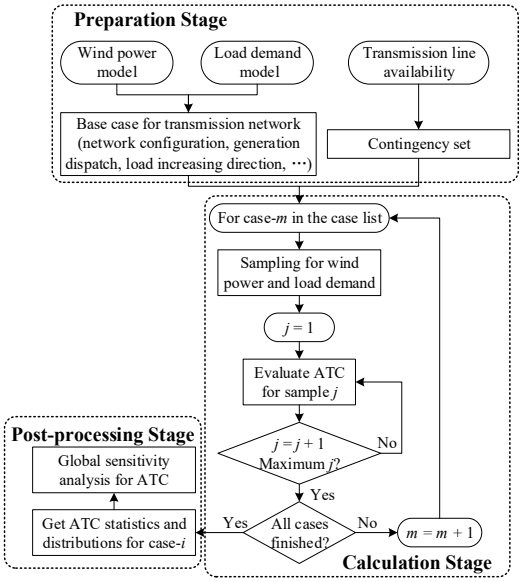

Fig. 2. *Proposed probabilistic ATC assessment procedure*

4.1. Preparation Stage

In the preparation stage, the uncertainties existing in system operation are modeled as random variables according to the historical or forecasted data available. There are two kinds of uncertainty sources considered in this paper.

The first category is the uncertainty of wind power or load demand which can be modeled as a continuous variable. While it is common practice to express uncertain customer behaviour, i.e., load increase rate/direction b_{D} in this study, as a Gaussian random variable, wind power uncertainty can be modeled in two ways. One is to first represent the wind speed v with a probability distribution like a Weibull distribution; then, active wind generation P_{W} is calculated by the energy conversion curve, i.e., $P_{\text{W}} = P_{\text{W}}(v)$. The other is to represent wind generation as a summation of its forecast value $P_{\text{W,f}}$ and the corresponding forecast error ε_{W}, i.e., $P_{\text{W}} = P_{\text{W,f}} + \varepsilon_{\text{W}}$, in which ε_{W} is subjected to a conditional probability distribution on $P_{\text{W,f}}$ and modeled as a Beta random variable or other suitable types.

The second category is the status or availability of transmission lines. The random line outage would cause a contingency that impacts ATC. Therefore, a set of contingency cases should be considered apart from the base case to ensure that the system can withstand the effects of the most restrictive line outage. In this paper, the contingency list is made by state enumeration until a termination rule, e.g., minimum contingency probability or maximum contingency

number. The probabilities of the base case C_0 and the contingency C_k are calculated as:

$$\begin{cases} \Pr(C_k) = \prod_{ij \in \boldsymbol{L}_a} (1-\gamma(ij)) \cdot \prod_{ij \in \boldsymbol{L}_{ua}} \gamma(ij) \\ \Pr(C_0) = 1 - \sum_{C_k \in \boldsymbol{CL}} \Pr(C_k) \end{cases} \tag{18}$$

where $\gamma(ij)$ is the outage rate of transmission line ij, $\boldsymbol{L_a}$ and $\boldsymbol{L_{ua}}$ are the collections of available lines and unavailable lines, respectively, and $\boldsymbol{CL}$ is the contingency set.

Contingencies concerning generator outages can be handled in a similar way. However, generator outage might cause the redispatch of generations and loads. As a result, the base case condition for the ATC will be changed.

According to the forecasted wind generations, load demands and facility status, a base case is defined based on the projected parameters concerning system configuration, generation dispatch, base scheduled transfers, etc. The load increase pattern and contingency are also specified for the next stage.

4.2. Calculation Stage

In the calculation stage, ATC is evaluated using the OPF model (3)~(11) for the base case at first. Then, the influence of uncertainties is addressed. For the base case and each contingency, wind generation $\boldsymbol{P}_W$ and load increment rate $\boldsymbol{b}_D$ are regarded as the input random variables, i.e., $\boldsymbol{X} = [\boldsymbol{P}_W; \boldsymbol{b}_D]$, of the OPF model whose LRA representation is constructed with a small number of model simulations. And then, the LRA is employed as the surrogate model to generate abundant ATC samples. The procedure is shown below.

Procedure of probabilistic ATC with LRA

For the base case and each contingency:

1. Generate the ED samples ($\boldsymbol{\xi}_{ed}$, $\boldsymbol{y}_{ed}$):
   a. Generate N_{ed} samples in the SRV space: $\boldsymbol{\xi}_{ed} = \{\boldsymbol{\xi}^{(1)}, \ldots, \boldsymbol{\xi}^{(Ned)}\}$;
   b. Transform $\boldsymbol{\xi}$ to $\boldsymbol{X}$ with the copula: $\boldsymbol{x}_{ed} = T^{-1}(\boldsymbol{\xi}_{ed})$;
   c. Evaluate the ATC responses through the OPF model: $\boldsymbol{y}_{ed} = \{y^{(1)}, \ldots, y^{(Ned)}\}$, $y^{(j)} = M(T^{-1}(\boldsymbol{\xi}^{(j)})) = M(\boldsymbol{x}^{(j)})$;
2. Build the LRA representation of the OPF model using ($\boldsymbol{\xi}_{ed}$, $\boldsymbol{y}_{ed}$);
3. Sample $\boldsymbol{\xi}$ extensively, e.g., N_{sp} (>> N_{ed}) samples, then employ the LRA as the surrogate model to evaluate the ATC response for all these samples.

After traversing the case list:

4. Store the LRA model and the ATC samples for all cases.

In the LRA-based method above, the OPF model is simulated $(1+k)\cdot N_{ed}$ times, where k is the size of the contingency set. If the same amount of ATC samples is generated, saying $(1+k)\cdot N_{sp}$, the total number of OPF executions N_{sim} would equate the $(1+k)\cdot N_{sp}$ in the MCS-based method. There are two reasons why it can significantly reduce the computation effort: (i) the number of OPF model simulations is reduced since N_{ed} is far less than N_{sp}; (ii) it takes negligible time to evaluate the ATC response through the surrogate model since only linear algebraic operations are involved.

4.3. Post-Processing Stage

In the post-processing stage, the probabilistic ATC are characterised. According to the law of total probability, the probability density function (PDF) of ATC is expressed as:

$$pdf(ATC) = \sum_{m=0}^{k} \rho(\boldsymbol{y}_m) \cdot \Pr(C_m) \tag{19}$$

where $\boldsymbol{y}_m$ is the ATC samples for the m-th case, and $\rho(\boldsymbol{y}_m)$ denotes the conditional density function of ATC fitted with $\boldsymbol{y}_m$.

The statistical moments, e.g., mean μ_{ATC} and variance σ^2_{ATC}, of ATC are calculated as:

$$\mu_{ATC} = \sum_{m=0}^{k} \mathrm{E}(\boldsymbol{y}_m) \cdot \Pr(C_m) \tag{20}$$

$$\sigma^2_{ATC} = \sum_{m=0}^{k} \mathrm{E}(\boldsymbol{y}_m^2) \cdot \Pr(C_m) - (\mu_{ATC})^2 \tag{21}$$

where E denotes the expectation of samples.

The probabilistic ATC calculation provides a range of ATC values with their probabilities instead of a deterministic value. Therefore, the probability-based or risk-based indices can be extracted and help system operators decide a proper ATC level [37]. For example, the TRM can be evaluated as:

$$TRM = ATC_0 - invcdf(\gamma) \tag{22}$$

where ATC_0 is calculated when the input random variables are set at the predicted values, *invcdf* denotes the inverse CDF of ATC, and γ is a percentile of the CDF specifying the risk level.

Furthermore, variance-based GSA makes up the second part of the post-processing stage. Its purpose is to quantify the importance of each random input on ATC variability, so that the most influential uncertainty sources are identified. For each case C_m, $m = 0, \ldots, k$, the GSI is defined by decomposing the variance of ATC into fractions which can be attributed to inputs or sets of inputs:

$$\begin{aligned} S_{m.i} &= \frac{\mathrm{Var}_{X_i}[\mathrm{E}_{X_{\sim i}}(Y_m \mid X_i)]}{\mathrm{Var}(Y_m)} \\ &= \frac{\mathrm{E}_{X_i}[(\mathrm{E}(Y_m)|X_i)^2] - (\mathrm{E}(Y_m))^2}{\mathrm{E}(Y_m^2) - (\mathrm{E}(Y_m))^2} \end{aligned} \tag{23}$$

where Var denotes the sample variance, $S_{m.i}$ denotes the GSI of the i-th input random variable X_i in the m-th case, Y_m is the ATC response, and $\boldsymbol{X}_{\sim i}$ is the sub-vector consisting of the variables in $\boldsymbol{X}$ except X_i.

The expression (23) can be estimated in a numerical way, with the stored LRA model [38], specifically:

$$\begin{aligned} \mathrm{E}(Y_m) &= \frac{1}{N_{gsa}} \sum_{j=1}^{N_{gsa}} \hat{M}_r(\boldsymbol{x}^{(j)}) \\ \mathrm{E}(Y_m^2) &= \frac{1}{N_{gsa}} \sum_{j=1}^{N_{gsa}} \hat{M}_r(\boldsymbol{x}^{(j)})^2 \\ \mathrm{E}_{X_i}[(\mathrm{E}(Y_m)|X_i)^2] &= \frac{1}{N_{gsa}} \sum_{j=1}^{N_{gsa}} [\hat{M}_r(\boldsymbol{x}^{(j)}) \cdot \hat{M}_r(x_i^{(j)}, \bar{\boldsymbol{x}}_{\sim i}'^{(j)})] \end{aligned} \tag{24}$$

where $\boldsymbol{x} = \{\boldsymbol{x}^{(1)}, \ldots, \boldsymbol{x}^{(Ngsa)}\}$ is sampled according to the joint PDF of $\boldsymbol{X}$, and $\bar{\boldsymbol{x}}'_{\sim i} = \{\bar{\boldsymbol{x}}'^{(1)}_{\sim i}, \ldots, \bar{\boldsymbol{x}}'^{(N_{gsa})}_{\sim i}\}$ is sampled according to the conditional PDF of $\boldsymbol{X}_{\sim i}$, when $X_i = x_i$.

Subsequently, $S_{m,i}$, $m = 0, \ldots, k$, are weighted to give the final sensitivity measure for the i-th input X_i:

$$S_i = \sum_{m=1}^{k} \left(\frac{\Pr(C_m)\mathrm{Var}(\boldsymbol{y}_m)}{\sigma^2_{ATC}} \right) \cdot S_{m.i} \tag{25}$$

The random inputs possessing larger weighted GSI values are supposed to have significant contributions to the

variability of ATC. Moreover, the sample size required in the numerical expression (24) is $N_{gsa}\cdot(2n+2)$ for all n input variables in each case. Since the ATC responses are evaluated by the LRA surrogate model, instead of solving the nonlinear OPF problem, the GSIs can be calculated in a shorter time than conventional methods.

5. Case Study

Numerical tests were carried out on a modified IEEE 118-bus system, whose basic parameters are available from the data files in ref. [39]. All tests were implemented in MATLAB on a PC with a 1.99-GHz Intel Core i7 and 16GB of RAM. The UQLab toolbox [40] was adopted for the construction of LRA and PCE.

The system is divided into two areas, as shown in Fig. 3, where Area-1 and Area-2 are the source area and sink area, respectively.

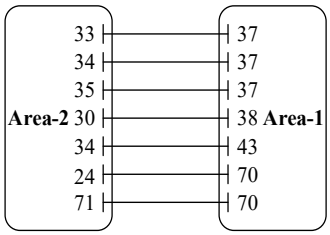

Fig. 3. *Decomposition of IEEE 118-bus system*

Twenty wind farms (WFs) of 100 MW each are connected to the network and replace conventional generators. These WFs are grouped into three sets, i.e., {1, 15, 18, 19, 32, 36}, {42, 46, 55, 56, 62}, and {70, 74, 76, 85, 91, 92, 104, 105, 110}. The normalised active wind generation is assumed to follow a Beta distribution. The associated parameters are α = 1.28, β = 2.97 for the first group, α = 2.63, β = 2.63 for the second group, and α = 3.78, β = 1.62 for the third group. In this paper, these parameters are selected according to ref. [41]. Moreover, the power outputs of WFs in the same group are supposed to be dependent and described by the Gaussian copula with a correlation coefficient of 0.5.

Besides wind power, the load increase rates are modeled as normally distributed variables. The mean value of normal variables is the active load demand in the base case, and the standard deviation is defined as 5% of the corresponding mean. The load increase rates are independent of each other.

Two test scenarios are designed as below:

Scenario S1: Only active wind generation is considered as random variables. The total number of random inputs is 20. This case is designed to study the impacts of wind power uncertainty on transmission ATC.

Scenario S2: Besides the WF outputs, the increase rates of loads with active powers greater than 10 MW are also assumed as random variables. The total number of random inputs is 110. This case is designed to test the capability of the proposed method in tackling high-dimensional problems.

5.1. ATC Assessment Without Considering Contingencies

In this study, only the uncertainties of load and wind powers are considered in the probabilistic ATC evaluation. In the proposed method, the LRA representation has been constructed with rank r = 1 and polynomial degree p_i = 2. In order to assess the LRA performance as a surrogate model, the relative generalisation error measure of model responses is calculated for the samples in the validation set:

$$err_G = [\frac{1}{N_{vld}}\sum_{i=1}^{N_{vld}}(atc_{sm}^{(i)} - atc_{om}^{(i)})^2] / \mathrm{Var}(\boldsymbol{atc}_{om}) \qquad (26)$$

where atc_{sm} and atc_{om} are the ATC responses evaluated by the surrogate model and the original model, respectively. N_{vld} is the size of the validation set, set as 1×10^4 in this study.

The LRA representations are built up separately under a range of ED sizes, varying from 1n to 10n where n is the number of input random variables. Because ED is generated randomly by simple random sampling (SRS), 100 trials of independent tests are conducted under each ED size. The maximum err_G and the average err_G curves versus the ED size N_{ed} are plotted in Fig. 4.

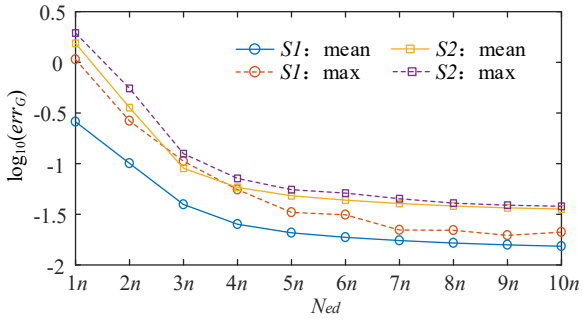

Fig. 4. *Error curves of the surrogate model in evaluating output response*

As indicated by the error curves, both the accuracy and robustness of LRA in evaluating ATC are improved with an increased ED size. However, further enrichment of ED samples contributes little to improve the performance of LRA above N_{ed} = 5n. Therefore, the LRA representations constructed with 100 ED samples for *scenario S1* and 550 for *scenario S2* are regarded as the *effective surrogate* models and adopted for the following probabilistic ATC evaluations.

Furthermore, the influence of parameters selected on the LRA performance is discussed. Under ED size N_{ed} = 5n, the err_G indexes of model built with different combinations of rank r and polynomial degree p_i are presented in Table 2. The increased rank or polynomial degree leads to more terms added into the LRA model, which would require enriched ED set to determine those unknown constants in subsequence. According to the results in the table, the combination of r = 1 and p_i = 2 produces a better surrogate model.

Table 2 Influence of parameters selected on surrogate model

		p_i = 1	p_i = 2	p_i = 3
S1	r = 1	2.00×10^{-2}	**1.54×10^{-2}**	1.92×10^{-2}
	r = 2	8.71×10^{-2}	6.48×10^{-2}	3.61×10^{1}
S2	r = 1	4.65×10^{-2}	**4.10×10^{-2}**	7.09×10^{-2}
	r = 2	2.41×10^{1}	1.65×10^{1}	3.57×10^{2}

1) Statistical and Probabilistic Results of ATC: The MCS-based probabilistic ATC results serve as the benchmark for assessing the accuracy of the proposed method in estimating statistics and probabilities of ATC. In MCS, 5000 times of the OPF-based simulations are conducted so that its result is converged. The statistical results of ATC provided

by LRA and MCS are listed in Table 3. The compared indices include the mean value μ, the standard deviation σ, and the inverse CDF value $invcdf_\gamma$ at cumulative probability γ.

Table 3 ATC statistics evaluated by two compared method

	method	μ / MW	σ / MW	$invcdf_{0.1}$ / MW	$invcdf_{0.5}$ / MW	$invcdf_{0.9}$ / MW
S1	MCS	737.67	82.08	637.83	728.46	852.24
	LRA	737.78	81.28	634.05	728.78	853.51
S2	MCS	607.14	47.33	547.64	605.85	669.29
	LRA	607.00	47.17	546.55	605.85	668.80

The results in the table above reveals that LRA with the *effective surrogate* model can give similar ATC statistics to those of MCS. This can attribute to that the surrogate model is statistically equivalent to the OPF model in estimating ATC. Even though the accuracy of LRA is proved.

The efficiency of the probabilistic ATC evaluation has been also evaluated and Table 4 presents the computation time cost by the proposed method. The total time cost t_{total} is divided into three parts, where t_{org} is consumed by evaluating actual ATC with the OPF model, t_{lra} is the cost by solving LRA constants, and t_{srg} is the time spent in assessing ATC by the surrogate model. In comparison, the MCS consumes more than 910 s to finish the whole simulation procedure in both scenarios.

Table 4 Time cost of LRA for the probabilistic ATC

	N_{ed}	t_{total} / s	t_{org} / s	t_{lra} / s	t_{srg} / s
S1	100	18.82	18.27	0.37	0.18
S2	550	101.51	100.49	0.80	0.22

As shown in Tab. 2, the time cost of LRA is only about 2% and 11% of MCS. The calculation time is reduced because the surrogate model is more efficient than the OPF model in yielding a large quantity of ATC outputs. Specifically, in *scenario S1*, it takes around 913.39 s through the OPF model and 0.18 s through the surrogate model for 5000 ATC simulations. Moreover, it also founds that the majority of the computational time is taken by t_{org}. Therefore, although it can improve the accuracy of the surrogate model partly by enriching the ED as shown in Fig. 3, more time cost for the probabilistic ATC evaluation is also expected.

2) Global Sensitivity Analysis of ATC: Taking *scenario S1* as an example, sensitivity analysis is performed in the post-processing stage. With expressions (23) and (24), it needs 1.1×10^4 ATC responses evaluated for 20 random inputs for the base case when setting $N_{gsa} = 500$. Two methods are compared here: (i) *PM* represents that ATC is assessed by the *effective surrogate*, and (ii) *CM* represents that ATC is evaluated by solving OPF. The absolute difference between the GSI values calculated in two ways is visualized in Fig. 5, which verifies that LRA is capable of estimating the right indices. Besides that, *PM* and *CM* cost 0.4 s and 33 min to finish the analysis, respectively. The advantage in efficiency highlights that LRA is a better choice for performing GSA.

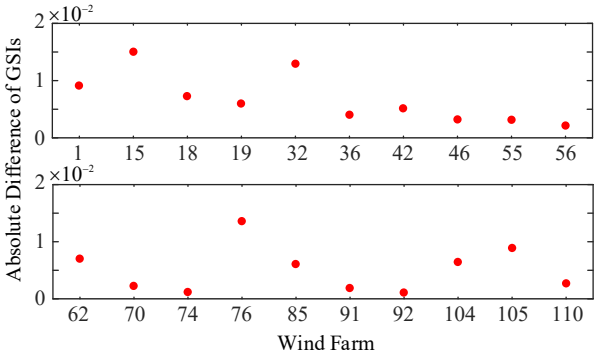

Fig. 5. *Absolute difference of GSI values calculated in two ways*

The GSA results reveal that six WFs in the first group are significantly important and dominate the ATC variability. The index values of other WFs are close to zero. It can be justified by looking at the OPF solution showing that the thermal limits of lines 5–8, 23–32 and 30–38 prevent further growth of the power exchange between areas. The important WFs identified are close to these critical paths, and their generation variation would have a more significant influence on the fluctuation of power carried by the critical lines, as well as the ATC variability.

Furthermore, the effects of correlation are also investigated, with wind generation supposed to be either dependent (*S1-dpt*) or independent (*S1-idpt*), respectively. Table 5 presents the GSIs for the influential WFs. In the independent case, even though the WFs are under the same marginal distribution, their levels of importance can differ from each other, as suggested by the distinct GSI values. However, once the correlated wind power is taken into account, it seems all these WFs have similar impacts on ATC variance.

Table 5 GSA results under different input conditions

	WF1	WF15	WF18	WF19	WF32	WF36
S1-dpt	0.606	0.579	0.612	0.609	0.582	0.470
S1-idpt	0.304	0.148	0.149	0.124	0.223	0.003

3) Comparison with the PCE-Based Method: The second-order sparse PCE is built up by least-angle regression [15] and used as the compared surrogate model. The study is conducted for *scenario S2*. For the same ED set, the err_G measures are evaluated for LRA and PCE, respectively. As shown in Fig. 6, LRA can achieve better accuracy when the ED size is relatively small, e.g., $N_{ed} < 12n$ here. However, the error of PCE decreases faster and would beat LRA when the ED size is large enough. The other attractive feature of LRA is that the time consumed for constructing the surrogate model remains approximately invariant as the ED size increases. In contrast, it takes much more time for PCE when the ED size is large. This is attributed to PCE involving the solution of a large-scale regression problem with the sparse technique, while a series of small-size regression problems are addressed by LRA when building up the surrogate model.

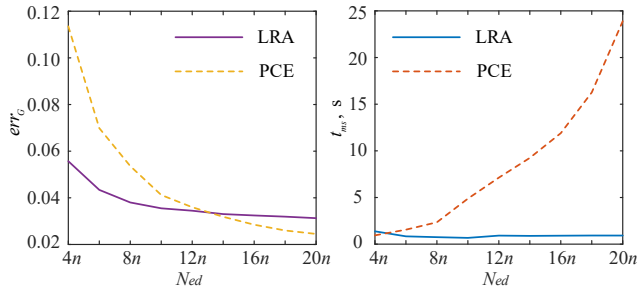

Fig. 6. *Accuracy and efficiency comparisons between LRA and PCE*

4) Comparison with the PEM-Based Method: With a classical PEM scheme, the total rounds of deterministic ATC simulations are 41 for *scenario S1* and 221 for *scenario S2*, which are less than LRA and MCS. It demonstrates the merit of efficiency of PEM as a small-sample method. Taking *scenario S2* as an example, the mean and standard deviation of ATC assessed by PEM are 607.10 MW and 47.54 MW respectively, which indicates that PEM and LRA have similar accuracy levels for calculating statistics of ATC. However, the performance of PEM evaluating probability distributions depends on the series expansion combined [42]. In contrast, not only the statistics but also probability distributions of ATC can be accurately estimated by the proposed method without using any series expansion. The CDFs of ATC generated by Gram-Charlier series (PEM-GCS) and Cornish-Fisher series (PEM-CFS), as well as MCS and LRA are plotted in Fig. 7. The CDF curves in the figure clearly demonstrate that LRA performs better than PEM in terms of probability distribution evaluations.

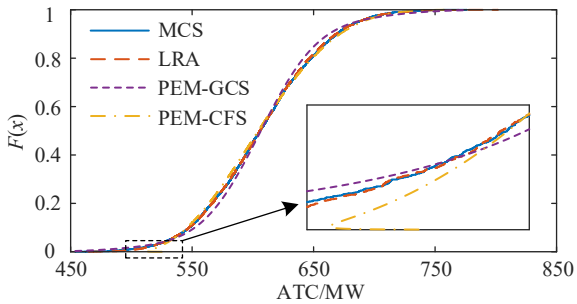

Fig. 7. *CDFs of ATC assessed by different methods*

5.2. ATC Assessment Including Contingencies

This study is conducted to validate the effectiveness of the proposed method in tackling contingencies and to investigate the effects of line outages on transfer capability. In *scenario S1*, eight contingencies are included in the ATC evaluation, i.e., the N-1 outage of lines 2–12, 11–13, 23–24, 25–27, 17–30, 26–30, 38–37 and 38–65. The contingency is selected in this way to lead to a remarkable reduction in ATC. In order to exhibit the impacts clearly, the probability of each contingency is set as $\Pr(C_i) = 0.005$, $i = 1, \ldots, 8$.

In MCS, the OPF model is simulated 5×10^4 times. In the proposed method, the LRA representations are constructed for the base case and eight contingency cases respectively. In each case, the OPF model is executed 900 times. The time consumed by the proposed method is only about 2% of that by the MCS. Besides saving computation effort, the proposed method can also provide an accurate estimation for probability distribution curves and statistics of ATC, as shown in Fig. 8 and Table 6.

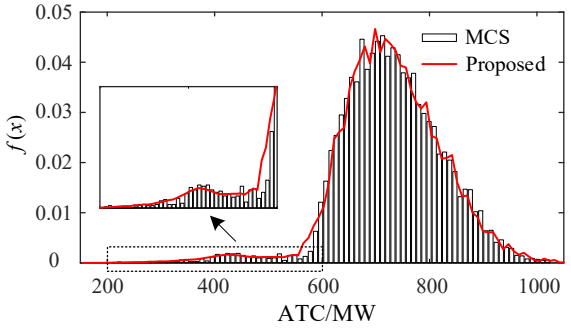

Fig. 8. *PDFs of ATC assessed by two methods*

Table 6 ATC statistics evaluated by two compared method

	μ / MW	σ / MW	$invcdf_{0.1}$ / MW	$invcdf_{0.5}$ / MW	$invcdf_{0.9}$ / MW
MCS	728.34	95.63	625.57	725.61	850.18
LRA	727.59	96.79	624.22	725.18	848.24

And then, the GSIs for WFs are calculated for each case involved and then weighted to assess the WF importance. As shown by Table 7, both the values and rankings of the weighted GSI of a WF are different under each case. For example, WF1 is recognized as the most influential one when line 2–12 or 17–30 is out of service, and WF15 is more contributory to the ATC variation when line 11–13 is in the outage.

Table 7 GSIs of WFs under the contingencies considered

	WF1	WF15	WF18	WF19	WF32	WF36
C_0/BASE	0.606	0.579	**0.612**	0.609	0.582	0.470
C_1/2–12	**0.986**	0.289	0.376	0.342	0.308	0.346
C_2/11–13	0.412	**0.797**	0.586	0.658	0.370	0.418
C_3/23–24	0.613	0.564	**0.664**	0.578	0.567	0.485
C_4/25–27	0.460	0.455	0.555	0.479	**0.806**	0.484
C_5/17–30	**0.729**	0.565	0.611	0.584	0.499	0.470
C_6/26–30	0.622	0.547	**0.667**	0.592	0.593	0.478
C_7/38–37	0.587	0.606	**0.654**	0.564	0.539	0.565
C_8/38–65	0.551	0.519	**0.645**	0.569	0.549	0.575
WEIGHTED	0.515	0.489	**0.519**	0.514	0.492	0.399

According to the weighted indices, WF1, 15, 18, 19, 32 and 36 are identified as the most significant uncertainty sources, while the other fourteen WFs are negligible as their GSIs are almost zero. This result can help to reduce the input random variables in the probabilistic ATC calculation. If only these six random variables are considered while setting the generation of the other fourteen WFs as constant at the forecast value, the probability distribution of ATC keeps almost unchanged, as illustrated in Fig. 9. This result confirms that the proposed weighted GSI is capable of identifying the most contributing variables.

Finally, the probabilistic ATC calculation results are applied to decide a proper ATC level for the test system. If the uncertain factors are disregarded and fixed at their forecasted values, the ATC is evaluated as 746.89 MW. Then, the uncertainty of wind power is incorporated into the TRM,

that is equal to 129.91 MW using definition (22) at $\gamma = 0.05$. This margin is reserved as a countermeasure to the power variation of WF1, 15, 18, 19, 32 and 36, as discussed before and, consequently, ATC is reduced to 616.98 MW. Furthermore, if random line outages are also taken into consideration, the reserved TRM increases to 145.79 MW and ATC reduces 601.10 MW to ensure system security.

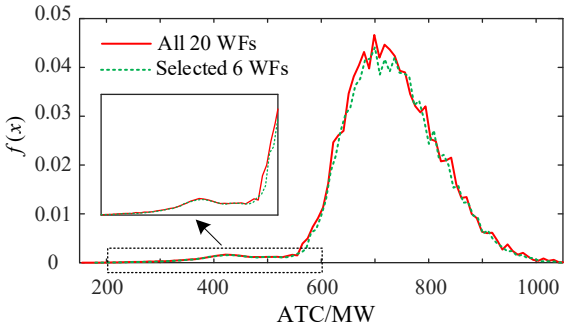

Fig. 9. *PDFs of ATC under different random input conditions*

6. Conclusion

This paper presents a novel probabilistic approach to evaluate ATC incorporating the uncertainties of load, wind power and transmission line failures. Numerical studies show that: 1) The proposed method can accurately and efficiently evaluate the probability distribution and statistics of ATC; 2) for high-dimensional problems LRA is better than either PCE or MCS, as it involves less computation effort while achieving comparable precision; 3) The weighted GSI provides a valid tool to identify the most influential random variables. The proposed method offers system operators a tool for deciding an appropriate ATC level for the transmission network.

References

[1] E. Ela and M. O'Malley, "Studying the variability and uncertainty impacts of variable generation at multiple timescales", IEEE Trans. Power Syst., 2012, 27, (3), pp. 1324–1333.

[2] Transmission Transfer Capability Task Force, "Available transfer capability definitions and determination", Princeton, NJ, USA: North American Electric Reliability Council, 1996.

[3] G. C. Ejebe, J. G. Waight, and M. Sanots-Nieto, et al, "Fast calculation of linear available transfer capability", IEEE Trans. Power Syst., 2000, 15, (3), pp. 1112–1116.

[4] A. J. Flueck, H. Chiang, and K. S. Shah, "Investigating the installed real power transfer capability of a large scale power system under a proposed multiarea interchange schedule using CPFLOW", IEEE Trans. Power Syst., 1996, 11, (2), pp. 883–889.

[5] M. H. Gravener and C. Nwankpa, "Available transfer capability and first order sensitivity", IEEE Trans. Power Syst., 1999, 14, (2), pp. 512–518.

[6] E. De Tuglie, M. Dicorato, and M. La Scala, et al, "A static optimization approach to assess dynamic available transfer capability", IEEE Trans. Power Syst., 2000, 15, (3), pp. 1069–1076.

[7] X. Fang, F. Li, and N. Gao, "Probabilistic available transfer capability evaluation for power systems including high penetration of wind power", 2014 International Conference on Probabilistic Methods Applied to Power Systems (PMAPS), 2014, pp. 1-6.

[8] P. Du, W. Li, and X. Ke, et al, "Probabilistic-based available transfer capability assessment considering existing and future wind generation resources", IEEE Trans. on Sustain. Energy, 2015, 6, (4), pp. 1263-1271.

[9] H. Chen, X. Fang, and R. Zhang, et al, "Available transfer capability evaluation in a deregulated electricity market considering correlated wind power", IET Gen. Trans. & Distri., 2018, 12, (1), pp. 53-61.

[10] Y. Liu, U. Zhao, and L. Xu, et al, "Online TTC estimation using nonparametric analytics considering wind power integration", IEEE Trans. on Power Syst., 2019, 34, (1), pp. 494-505.

[11] A. M. Leite Da Silva, J. G. De Carvalho Costa, and L. A. Da Fonseca Manso, et al, "Transmission capacity: availability, maximum transfer and reliability", IEEE Trans. on Power Syst., 2002, 17, (3), pp. 843-849.

[12] A. B. Rodrigues, M. G. Da Silva, "Probabilistic Assessment of Available Transfer Capability Based on Monte Carlo Method With Sequential Simulation", IEEE Trans. on Power Syst., 2007, 22, (1), pp. 484-492.

[13] A. Berizzi, C. Bovo, and M. Delfanti, et al, "A Monte Carlo approach for TTC evaluation", IEEE Trans. on Power Syst., 2007, 22, (2), pp. 735-743.

[14] M. Ramezani, C. Singh, and M. Haghifam, "Role of clustering in the probabilistic evaluation of TTC in power systems including wind power generation", IEEE Trans. on Power Syst., 2009, 24, (2), pp. 849-858.

[15] G. Luo, J. Chen, and D. Cai, et al, "Probabilistic assessment of available transfer capability considering spatial correlation in wind power integrated system", IET Gen. Trans. & Distri., 2013, 7, (12), pp. 1527–1535.

[16] N. F. Avila, and C. Chu, "Distributed probabilistic ATC assessment by optimality conditions decomposition and LHS considering intermittent wind power generation", IEEE Trans. on Sustain. Energy, 2019, 10, (1), pp. 375-385.

[17] E. Haesen, C. Bastiaensen, and J. Driesen, et al, "A Probabilistic formulation of load margins in power systems with stochastic generation", IEEE Trans. Power Syst., 2009, 24, (2), pp. 951–958.

[18] G. Luo, X. Wu, and G. Wu, et al, "A stochastic response surface method for probabilistic assessment of ATC in wind

power integrated system", 2018 IEEE Power & Energy Society General Meeting (PESGM), Portland, OR, 2018, pp. 1-5.

[19] X. Sun, Q. Tu, and J. Chen, et al, "Probabilistic load flow calculation based on sparse polynomial chaos expansion", IET Gen., Trans. & Distri., 2018, 12, (11), pp. 2735-2744.

[20] C.-L. Su and C.-N. Lu, "Two-point estimate method for quantifying transfer capability uncertainty", IEEE Trans. Power Syst., 2005, 20, (2), pp. 573–579.

[21] M. M. Othman, A. Mohamed, and A. Hussain, "Determination of transmission reliability margin using parametric bootstrap technique", IEEE Trans. Power Syst., 2008, 23, (4), pp. 1689–1700.

[22] M. Fan, V. Vittal, and G. H. Heydt, et al, "Probabilistic power flow studies for transmission systems with photovoltaic generation using cumulants", IEEE Trans. on Power Syst. 2012, 27, (4), pp. 2251-2261.

[23] R. Preece, and J. V. Milanović, "Assessing the applicability of uncertainty importance measures for power system studies", IEEE Trans. Power Syst., 2018, 31, (3), pp. 2076–2084.

[24] X. Li, D. Hui and X. Lai, "Battery energy storage station (BESS)-based smoothing control of photovoltaic (PV) and wind power generation fluctuations", IEEE Trans. on Sustain. Energy, 2013, 4, (2), pp. 464-473.

[25] R. Preece, J. V. Milanovic, "Assessing the applicability of uncertainty importance measures for power system studies", IEEE Trans. on Power Syst., 2016, 31, (3), pp. 2076-2084.

[26] I. M. Sobol, "Global sensitivity indices for nonlinear mathematical models and their Monte Carlo estimates", Math. and Comput. in Simul., 2001, 55(1-3), pp. 271-280.

[27] T. G. Kolda and B. W. Bader, "Tensor decompositions and applications," SIAM Rev., 2009, 51, (3), pp. 455–500.

[28] G. Beylkin, J. Garcke, and M.J. Mohlenkamp, "Multivariate regression and machine learning with sums of separable functions", SIAM J. Sci. Comput., 2009, 31, (3), pp. 1840–1857.

[29] A. Doostan, A. Validi, and G. Iaccarino, "Non-intrusive low-rank separated approximation of high-dimensional stochastic models", Comput. Methods Appl. Mech. Eng., 2013, 263, (17), pp. 42–55.

[30] M. Chevreuil, R. Lebrun, and A. Nouy, et al, "A least-squares method for sparse low rank approximation of multivariate functions", SIAM/ASA J. Uncertain. Quantificat., 2015, 3, (1), pp. 897–921.

[31] H. Sheng, and X. Wang, "Probabilistic power flow calculation using non-intrusive low-rank approximation method", IEEE Trans. on Power Syst., 2019, 34, (4), pp. 3014-3025.

[32] K. Konakli and B. Sudret, "Polynomial meta-models with canonical low-rank approximations: Numerical insights and comparison to sparse polynomial chaos expansion", J. Comput. Phys., 2016, 321, pp. 1144–1169.

[33] Y. Ou and C. Singh, "Assessment of available transfer capability and margins", IEEE Trans. Power Syst., 2002, 17, (2), pp. 463–468.

[34] D. Gan, R. J. Thomas, and R. D. Zimmerman, "Stability-constrained optimal power flow", IEEE Trans. on Power Syst., 2000, 15, (2), pp. 535-540.

[35] G. Papaefthymiou and D. Kurowicka, "Using copulas for modeling stochastic dependence in power system uncertainty analysis", IEEE Trans. Power Syst., 2009, 24, (1), pp. 40–49.

[36] D. Xiu, "Numerical Methods for Stochastic Computations: A Spectral Method Approach", Princeton, NJ, USA: Princeton University Press, 2010, pp. 25–30.

[37] J. McCalley, et al, "Probabilistic security assessment for power system operations", IEEE Power Eng. Soc. General Meeting, Denver, CO, USA, 2004, 1, pp. 212–220.

[38] K. Konakli and B. Sudret, "Global sensitivity analysis using low-rank tensor approximations", Reliab. Eng. Sys. Safety, 2016, 156, pp. 64–83.

[39] R. D. Zimmerman, C. E. Murillo-Sanchez, and R. J. Thomas, "MATPOWER: steady-state operations, planning and analysis tools for power systems research and education", IEEE Trans. Power Syst., 2011, 26, (1), pp. 12–19.

[40] S. Marelli and B. Sudret, "UQLab: A framework for uncertainty quantification in MATLAB", Proc. 2nd Int. Conf. Vulnerability, Risk Analysis and Management, Liverpool, United Kingdom, 2014, pp. 2554–2563.

[41] A. Fabbri, T. G. S. Roman, and J. R. Abbad, et al, "Assessment of the cost associated with wind generation prediction errors in a liberalized electricity market", IEEE Trans. on Power Syst., 2005, 20, (3), pp. 1440-1446.

[42] Z. Ren, W. Li, and R. Billinton, et al, "Probabilistic power flow analysis based on the stochastic response surface method", IEEE Trans. Power Syst., 2016, 31, (3), pp. 2307–2315.